Illumination correction of retinal images using Laplace interpolation

Conor Leahy,[1,*] Andrew O'Brien,[1] and Chris Dainty[1,2]

[1]Applied Optics Group, School of Physics, National University of Ireland, Galway, Ireland

[2]Blackett Laboratory, Imperial College, London SW7 2BZ, UK

*Corresponding author: conor.leahy@nuigalway.ie

Received 13 September 2012; revised 4 November 2012; accepted 6 November 2012; posted 7 November 2012 (Doc. ID 176201); published 6 December 2012

Retinal images are frequently corrupted by unwanted variations in intensity that occur due to general imperfections in the image acquisition process. This inhomogeneous illumination across the retina can limit the useful information accessible within the acquired image. Specifically, this can lead to serious difficulties when performing image processing tasks requiring quantitative analysis of features present on the retina. Given that the spatial frequency content of the shading profile often overlaps with that of retinal features, retrospectively correcting for inhomogeneous illumination while maintaining the radiometric fidelity of the real data can be challenging. This paper describes a simple method for obtaining an estimate of the illumination profile in retinal images, with the particular goal of minimizing its influence upon features of interest. This is achieved by making use of Laplace interpolation and a multiplicative image formation model.

OCIS codes: 100.0100, 170.3880.

1. Introduction

Automatic feature extraction from retinal images is an important tool in clinical research. Retinal images are commonly affected by inhomogeneous illumination (or "shading") [1,2]. This can be caused by, e.g., imperfections in the imaging optics, spatial inhomogeneity of the illuminating light source, light from nonuniformities in the human cornea or lens, natural vignetting, or artificial vignetting (due to misalignment of the subject's eye). The result is that the acquired images contain nonuniformities of illumination, manifested as low-frequency spatial variations in contrast and luminosity across the image [3]. Furthermore, extended features, such as the blood vessels, fovea, and optic disc naturally have spatial variation in absorption of the illuminating light, which may be difficult to distinguish from shading. These effects can be seriously detrimental to any intended quantitative diagnostic task. The mitigation of shading effects is therefore of high importance when performing diagnostic tasks, particularly when feature extraction is one of the ultimate goals.

There are many different approaches to the correction of inhomogeneous illumination. These can be broadly classed into nonparametric methods (such as linear filtering, homomorphic filtering, and morphological analysis) and parametric methods (which typically employ polynomial fitting to obtain an estimate of the illumination profile). These methods attempt to recover the shading-free image from the original acquired image. A simple formulation is to regard the acquired image as equivalent to a shading-free image that has been corrupted by additive and/or multiplicative interference. For simplicity it is common to consider just the additive or the multiplicative mechanism alone [4].

An effective illumination correction method should remove the global shading from the image without corrupting features within the image. Methods based on spatial filtering have the advantage of simple

1559-128X/12/358383-07$15.00/0

implementation, but tend to perform poorly in situations where the shading function and retinal features within the true image have overlapping spatial frequency content. For retinal images, this occurs under relatively common conditions, and so filtering methods cannot be relied upon to perform illumination correction of retinal images without detrimentally affecting areas of the retinal image that may be required for diagnostics. Parametric methods based on polynomial fitting overcome this problem by using a set of node points within the image that are determined to be representative only of the image background, and not of any features. This is typically achieved by using some local measure of structure, such as the coefficient of variation [5,6]. Such methods tend to perform less well when large features are present in the image [4]. These methods also tend to employ low-order polynomials in order to obtain a smooth correction, but this may lead to poor correction at the edges of an image, where there is often a pronounced variation in illumination due to vignetting [1]. Likar *et al.* [2] presented an approach based on entropy minimization that estimated both an additive and a multiplicative term. This was shown to perform well for a variety of images, though it also relies on polynomial fitting and as such is subject to some of the same associated issues as other polynomial fitting methods. A method proposed by Kubecka *et al.* [7] also employed entropy minimization as the quality criterion, with a B-spline multiplicative image formation model. The authors derived analytical expressions for the derivative of the entropy, so as to enable optimization routines to be employed efficiently for the minimization.

Image inpainting is a term commonly used to refer to techniques for filling in regions of missing data within images [8]. The basic principle is to replace the missing data using information from its surroundings, and is achieved using interpolation [9]. The technique can be employed to remove prominent features from an image in such a manner as to have minimal noticeable effect on the background. A partial differential equation (PDE) is typically used to automate this interpolation process [10]. The implementation of inpainting techniques requires a mathematical representation of the image (in our case this is available in the form of grayscale pixel values) and a suitable choice of PDE to govern the replacement of missing pixels.

In this paper, a novel method of correcting inhomogeneous illumination in retinal images is presented. The method makes use of image inpainting, and is specifically intended for diagnostic applications whereby extended features are to be extracted from the image for quantitative analysis. As such, great care is taken to preserve features within the image and to avoid their obscuration at all costs during the correction process. This is in contrast to other methods that attempt to maximize the visual quality of the image for the purpose of qualitative analysis or image registration. We present results in the form of illumination correction performed on narrow-field images obtained from a retinal imaging system, and compute a metric of the effectiveness of the correction.

2. Methods

Retinal images were obtained using a bespoke fundus camera. The camera operated with Maxwellian view, with a 3 mm operating pupil. The image sensor was a 12 bit monochrome CCD type. The image field size was approximately 12° on the retina. At acquisition time, the imaging was centered on the foveal region by use of a fixation target. Two different illumination sources were used alternately: a blue LED (typical peak wavelength $\lambda_p = 470$ nm), and a green LED ($\lambda_p = 530$ nm). The LED sources were arranged in a ring for off-axis illumination.

A. Image Model

For each acquired image we attempt to recover an estimate of the true (i.e., shading-free) reflectance image $I_t(x,y)$. The true image is assumed to be a result of the interaction between a uniform illumination source and the object of interest. In our case, $I_t(x,y)$ is the reflectance measured from the retina. $I_t(x,y)$ cannot be measured directly, and so must be inferred from the acquired image obtained using the (imperfect) optical system. We refer to this as the acquired or shaded image $I(x,y)$. The problem of correcting inhomogeneous illumination is therefore to obtain an estimate of $I_t(x,y)$ from $I(x,y)$. For our purposes we assume that the inhomogeneous illumination is characterized by some smooth multiplicative function $U(x,y)$, and thus the shaded and shading-free images are related by

$$I(x,y) = U(x,y)I_t(x,y). \tag{1}$$

The problem of estimating $I_t(x,y)$ therefore reduces to finding a suitable estimate of $U(x,y)$ and then inverting the model. The estimate should be a smooth function, as shading effects are typically slow-varying across the image [4].

B. Removal of Retinal Features

The method of estimating $U(x,y)$ first necessitates removing from the image any prominent foreground features, particularly those that are of interest for subsequent diagnostic tasks. This requires the localization of these features within the retinal image. There is a wealth of literature devoted to automatic localization in digital retinal images of blood vessels [11–13], as well as other retinal features such as the fovea and the optic disc [14,15]. For this reason, we do not cover the topic here, but rather assume that the locations of all such features within $I(x,y)$ are available. Pixels corresponding to retinal features are masked to yield an initial estimate $\hat{U}(x,y)$ of $U(x,y)$ that contains undefined values.

C. Laplace Interpolation

To replace the missing values of the estimate $\hat{U}(x,y)$, an inpainting procedure is applied. This is performed by solving Laplace's equation:

$$\nabla^2 U = 0, \tag{2}$$

which, for an image can be written as:

$$\frac{\partial^2 U}{\partial x^2} + \frac{\partial^2 U}{\partial y^2} = 0. \tag{3}$$

Laplace's equation is a natural choice for the interpolating PDE as it minimizes the integrated square of the gradient,

$$\iint_{\Omega} |\nabla U(x,y)|^2 \mathrm{d}x\mathrm{d}y, \tag{4}$$

where $\nabla = [\partial/\partial x, \partial/\partial y]$ is the gradient operator and Ω is the region of interest within the image definition domain. Therefore, the solutions tend to be smooth, which is a desirable condition for estimation of the typically slow-varying shading function [16,17].

The solution of Eq. (2) is performed by applying the finite difference method, where the solution region is defined by the extent of the image. The finite difference method is a numerical technique for the approximate solution of differential equations, given a solution region and boundary and/or initial conditions [18]. The representation of the image in pixels lends itself naturally to the division of the solution region into a grid of nodes suitable for utilizing finite differences. The boundary conditions are formed from the known pixels within the image; this is known as a Dirichlet problem [19]. Indeed, the boundary conditions do not just consist of values at the edge of the image, but there are typically also many "internal" boundary conditions in the form of the known (i.e., unmasked) pixel values elsewhere within the image [17].

The solution region is divided into a grid of nodes (which are generalized to pixels in this case), and the differential equation (in this case Eq. (3)) is then approximated by a set of linear algebraic equations on the pixels within the solution region. This set of algebraic equations is then solved using an implicit method.

Approximating the derivatives at a pixel (x_0, y_0) gives

$$\left.\frac{\partial^2 U}{\partial x^2}\right|_{x=x_0} \approx \frac{U(x_0+\Delta x, y_0) - 2U(x_0,y_0) + U(x_0-\Delta x, y_0)}{(\Delta x)^2}, \tag{5}$$

$$\left.\frac{\partial^2 U}{\partial y^2}\right|_{y=y_0} \approx \frac{U(x_0, y_0+\Delta y) - 2U(x_0,y_0) + U(x_0, y_0-\Delta y)}{(\Delta y)^2}, \tag{6}$$

where $\Delta x = \Delta y$ is the (square) pixel size. Substituting into Eq. (3) and simplifying notation, we can write

$$\hat{U}_0 = \frac{1}{4}(U_u + U_d + U_l + U_r), \tag{7}$$

where $\hat{U}_0$ denotes the shading estimate at any particular missing pixel (apart from at the boundary of the image), and the subscripts u, d, l, r denote the adjacent pixels ("up," "down," "left," and "right"). This is illustrated in Fig. 1. It is clear from Eq. (7) that applying Laplace's equation to the inpainting problem can effectively be interpreted as a differential means of stating that the value of a given missing pixel is modelled as an average of the adjacent pixel values [18]. At the boundary of the image, all four adjacent pixels are not available, and so special cases of Eq. (7) incorporating only pixels within or on the boundary are required [17].

Using Eq. (7), one obtains a system of linear equations with one equation for each missing pixel. These are solved using a matrix equation of the form [18]:

$$\mathbf{Ax} = \mathbf{b}, \tag{8}$$

where $\mathbf{A}$ is a square band matrix of coefficients, $\mathbf{x}$ is a column vector of unknown pixel values, and $\mathbf{b}$ is a column vector of the known pixel values. The unknown pixel values can then be obtained by solving

$$\mathbf{x} = \mathbf{A}^{-1}\mathbf{b}. \tag{9}$$

The missing values of the shading function estimate can then be extracted from $\mathbf{x}$ to complete the $\hat{U}(x,y)$ function.

D. Correction

Once the inpainting procedure is concluded, a complete representation of the shading function estimate $\hat{U}(x,y)$ is available. The shading-free image can thus be estimated as follows:

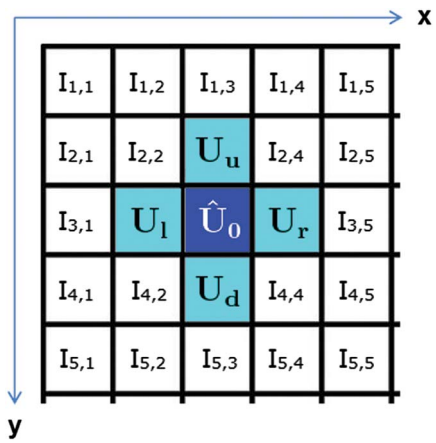

Fig. 1. (Color online) Illustration of Laplace interpolation as given by Eq. (7).

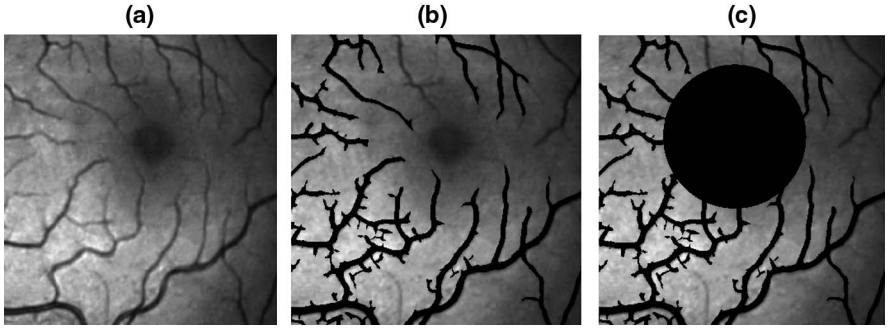

Fig. 2. (a) Original acquired image, (b) image with vascular detail masked, and (c) image with both vascular detail and the foveal region masked.

$$\hat{I}_t(x,y) = \alpha \frac{I(x,y)}{\hat{U}(x,y)} + \beta, \tag{10}$$

where α and β are constant values that can be chosen so as to normalize the distribution of pixel values of $\hat{I}_t(x,y)$ to within the same range as that of the true image [3].

To evaluate the performance of the illumination correction, we make use of a luminosity metric proposed by Foracchia *et al.* [3]. The acquired and corrected images are first adjusted to have histograms with the same mean and standard deviation, using an affine transformation. The images are then split into a 10×10 grid of subimages. We then compute a metric σ_μ of nonuniformity throughout the image:

$$\sigma_\mu = \sqrt{\frac{1}{N}\sum_k (\mu_k - \mu_0)^2}, \tag{11}$$

where N denotes the number of pixels in each subimage, μ_k is the mean pixel value of the kth subimage, and

$$\mu_0 = \frac{1}{N}\sum_k \mu_k. \tag{12}$$

A lower σ_μ value is associated with more uniform image luminosity, and thus it is expected that a successful illumination correction should be associated with a reduction in the value of σ_μ.

3. Results

Figure 2(a) shows an example of a typical image acquired using blue illumination. The image features include both vascular structure and the fovea (which is highlighted). The image contains visible nonuniformity of illumination, with significantly higher luminosity in the lower-left portion of the image.

A. Removal of Retinal Features

The vascular detail was identified and removed from the image using a method similar to that described by Chanwimaluang *et al.* [11]. The foveal region was localized using a matched filter technique with an inverted Gaussian-shaped kernel [14]. The foveal region appears dark largely due to the presence of macular pigment, which strongly absorbs blue wavelengths [20]. We regard this darkened area as part of a single retinal feature including the fovea, and thus a large circular area must be masked. Figure 2(b) shows the original image with the vascular detail identified and masked (note that not all vessels were correctly identified; this may be symptomatic of the nonuniform illumination). Figure 2(c) shows the image with both vascular detail and the foveal region removed.

B. Laplace Interpolation and Correction

The remaining (unmasked) data within Fig. 2(c) is set as the estimate of the shading function, i.e., $\hat{U}(x,y)$. The missing values of $\hat{U}(x,y)$ are then found by Laplace interpolation. For each undefined pixel value of $\hat{U}(x,y)$, a corresponding equation was obtained using Eq. (7). The equations were then rearranged and assembled into the form of Eq. (9). The solution vector $\mathbf{x}$ gives the missing values of $\hat{U}(x,y)$, thus completing the shading function estimate. A median filter was then applied in order to further smoothen $\hat{U}(x,y)$. Figure 3(a) shows the shading function corresponding to the above example. The estimate $\hat{I}_t(x,y)$ of the shading-free image was then obtained using Eq. (10). Figure 3(b) shows $\hat{I}_t(x,y)$ for the example described above. The computed value

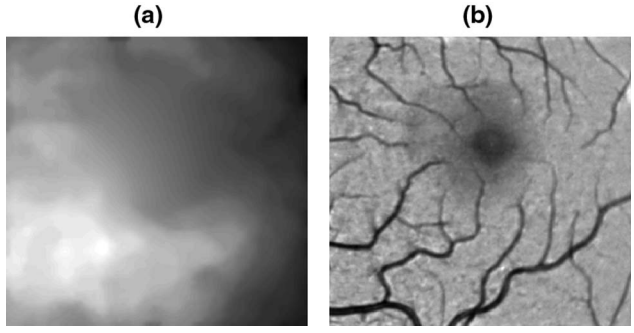

Fig. 3. (a) Shading function estimate $\hat{U}(x,y)$, after applying the Laplace interpolation procedure and additional smoothing. (b) Estimate of the shading-free image obtained after applying illumination correction.

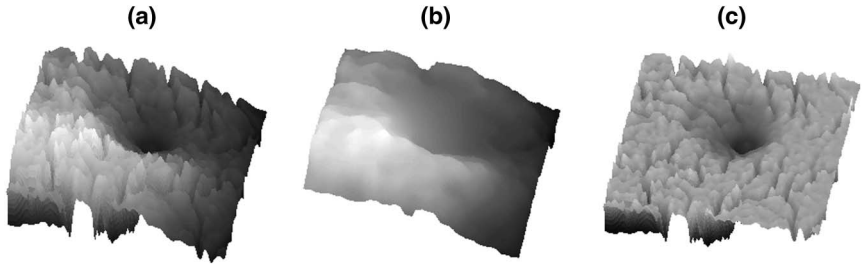

Fig. 4. 3D projection of: (a) the original acquired image, (b) the estimate of the shading function, and (c) the estimate of the shading-free image. The z dimension corresponds to grayscale pixel value. The figures are displayed with 15° horizontal rotation about the z-axis and 60° vertical elevation of the viewpoint.

of the nonuniformity metric σ_μ was 0.056 for the corrected image $\hat{I}_t(x,y)$, compared to 0.067 for the original image. This represents a reduction of 16.4%. Figure 4 shows three-dimensional projections of the original acquired image $I(x,y)$, along with the shading function estimate $\hat{U}(x,y)$, and the resultant shading-free image $\hat{I}_t(x,y)$. Figure 5 shows results for three different retinal images. In each case, the vascular structure and foveal region were masked in a similar manner to the example of Fig. 2, and

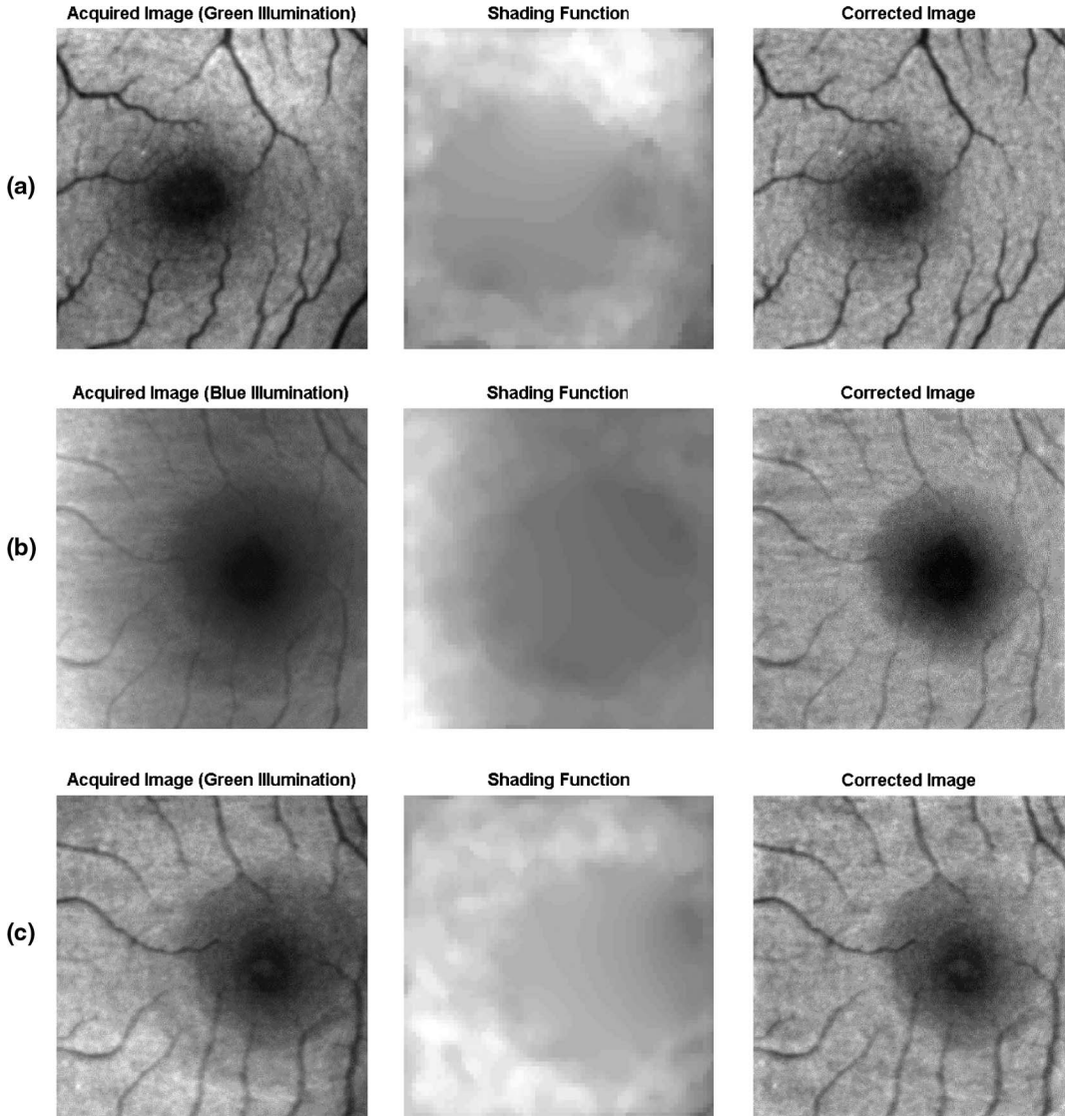

Fig. 5. Shading correction results for three retinal images: (a) Green illumination, acquired image $\sigma_\mu = 0.084$, corrected image $\sigma_\mu = 0.071$ (15.5% reduction). (b) Blue illumination, acquired image $\sigma_\mu = 0.128$, corrected image $\sigma_\mu = 0.111$ (13.3% reduction). (c) Green illumination, acquired image $\sigma_\mu = 0.082$, corrected image $\sigma_\mu = 0.071$ (13.4% reduction).

Laplace interpolation was then applied to obtain the estimate of the shading function and the subsequent corrected image.

4. Discussion

The amount of retinal features in an image is directly related to the number of pixels that must be masked, and consequently the required computational effort for the shading function estimate. It is important to be thorough when removing the features however, as remnants of partially masked features may be undesirably diffused by the interpolation procedure. For the foveal region, where there is typically a significant darkening of the image, the size of the masked portion should be chosen conservatively. The size of the fovea is typically around 5° on the retina [21], but the extent of the visibly darkened region in the reflectance image may be larger and varies from subject to subject. When masking the fovea, one should attempt to delete a portion that slightly exceeds the full extent of the darkened region. The accuracy of interpolating over such a large region may be called into question, but it should be remembered that the use of Laplace's equation ensures a smooth solution across the image, thus keeping the shading function estimate well-behaved even when large regions must be interpolated.

The optical system used to obtain the retinal images was originally developed for small-field images of approximately 12°. For larger field images, other retinal features such as the optic disc may be encompassed. These would need to be similarly detected and masked, as described in Subsection 2.B. The computational effort required to implement the algorithm on large-field images may increase, depending on the total number of masked pixels (and thus the number of unknowns in Eq. (9). The narrow-field images presented in this paper encompass the fovea, and so the ratio of retinal features to structureless regions is quite high. A 30°–40° retinal image, for example, would be likely to have a lower such ratio, and thus with more information available from structureless regions of the retina, the accuracy of the method could potentially be improved in that case.

A limitation of using Laplace's equation as the interpolating PDE is that an estimated pixel can never take a value above or below that of all its adjacent pixels. This can be resolved, for example, by instead solving the biharmonic equation, $\nabla^4 I = 0$. This effectively incorporates a larger neighborhood of pixels into the interpolation process. As described by Tobler and Kennedy [16], the resultant difference equation would be akin to an amendment of Eq. (7) to include 12 terms on the right-hand side instead of 4, thus representing a significant increase in complexity. Schönlieb [10] demonstrated inpainting based on the two-dimensional heat equation, as well as the use of a nonlinear diffusion technique to improve the preservation of discontinuities (such as edges) within the image. This technique utilized a fourth-order PDE and was shown to improve the inpainting outcome, but the author noted that to apply it with implicit methods would be computationally prohibitive.

Solving the inpainting problem using a band matrix method such as given in Eq. (9) can be computationally intensive if the image contains a large proportion of features compared to background pixels. For this reason, one may be tempted to use an iterative finite difference method approach to solving the inpainting problem [10,16]. This approach requires that the values of undetermined pixels be set to some initial guess, and then Eq. (7) is applied iteratively to each pixel. This iterative approach may be quicker than finding an implicit solution if not many iterations are required, but it also has the disadvantage that some stopping condition (e.g., a stability criterion) must be preset before the iteration process [18]. Alternatively, a solution to Eq. (9) can be found with less computational effort by exploiting the sparse structure of the band matrix. The inversion process can be greatly expedited by using, for example, the biconjugate gradient method with a sparse matrix storage format [17]. The shading correction algorithm was implemented on an Intel Xeon 2 GHz system with 2 GB RAM, using code written in MATLAB. Using an efficient sparse algebra approach (as suggested by D'Errico [22]), typical implementation times for 12°, 380×380 pixel retinal images were in the range of 4–5 s, of which 3–4 s were devoted to localization of the vascular detail and fovea. Given the wide availability of algorithms for detection of retinal features in the literature, we believe there is significant room for improvement on the obtained implementation times.

Distinguishing between true inhomogeneous illumination and natural spatial reflectance differences of the retina is challenging. The exclusion of pixels corresponding to the foveal region of the retina described in Subsection 2.B is a targeted effort to prevent the naturally lower reflectivity of this region from compromising the shading estimation. Determining the true extent of the darkened region is nontrivial however, as the spatial profile of macular pigment varies from person-to-person [23]. Thus, the separation between the foveal region and the rest of the image, as employed by the algorithm described in this work, is an approximation. This may lead to poor accuracy of the shading estimation in the foveal region. Some evidence of this can be seen in Fig. 5, where the shading function estimates exhibit darkening around the region corresponding to the fovea. This inaccuracy may be of less importance for larger images, where the size of deleted pixel regions would be smaller compared to the total image field size.

Evaluating the performance of a shading correction method is nontrivial, as suitable metrics are difficult to define [4]. In this work we made use of a metric of luminosity nonuniformity. For each of the images presented, the metric showed that the correction procedure reduced the degree of

nonuniformity in the image, as expected. The metric provides a simple method of comparing shaded and shading-free images, however it does not provide any information on the overlap between the spatial frequency content of the different object classes within the image. The coefficient of variation (computed as the standard deviation of pixel values divided by the mean) has also been used to assess the reduction in inhomogeneity after shading correction [24]. Likar *et al.* suggested a method of comparing the performance of correction on object classes within images, using a metric computed from the mean values and standard deviations of specifically chosen pixel regions [25]. The most meaningful image quality measures are in many cases based on visual assessment [26], therefore it may be valuable to develop metrics of shading correction performance that correlate well with subjective visual assessments of images.

In this work, we have presented a technique for correcting inhomogeneous illumination of retinal images aimed at applications where quantitative analysis of retinal features is the ultimate goal. As such, the approach is designed to maximize the radiometric fidelity of features within the image. This is achieved by comprehensively excluding the retinal features themselves from the estimation of the shading function. The method ensures that spatial frequency overlap of features and the image background (a common difficulty with other techniques [4]) is not an issue. The estimated shading function is necessarily smooth, which facilitates the inversion of the image formation model. The method lends itself well to automation and the use of the finite difference method means that the resulting problem is sparse, giving potential for a computationally efficient solution. This work may be of interest for the quantitative analysis of retinal features, such as the determination of blood oxygen levels within retinal vessels, or multispectral analysis of retinal pigments.

The authors would like to acknowledge several colleagues for helpful suggestions and discussions throughout the course of this work: Dr. Derek Coburn, Dr. Elizabeth Daly, Dr. Nicholas Devaney, and Dr. Andrew Lambert. This research was supported by Science Foundation Ireland Grant Number 07/IN.1/I906 and Enterprise Ireland.

References

1. L. Kubecka, R. Kolar, J. Jan, and R. Jirik, "Retrospective illumination correction of retinal images," presented at Eurasip Biosignal, Brno, Czech Republic, 28–30 June 2006.
2. B. Likar, J. B. A. Maintz, M. A. Viergever, and F. Pernuŝ, "Retrospective shading correction based on entropy minimization," J. Microsc. **197**, 285–295 (1999).
3. M. Foracchia, E. Grisan, and A. Ruggeri, "Luminosity and contrast normalization in retinal images," Med. Image Anal. **9**, 179–190 (2005).
4. D. Tomaževiĉ, B. Likar, and F. Pernuŝ, "Comparative evaluation of retrospective shading correction methods," J. Microsc. **208**, 212–223 (2002).
5. L. Leistritz and D. Schweitzer, "Automated detection and quantification of exudates in retinal images," Proc. SPIE **2298**, 690 (1994).
6. D. Schweitzer, S. Jentsch, J. Dawczynski, M. Hammer, U. E. K. Wolf-Schnurrbusch, and S. Wolf, "Simple and objective method for routine detection of the macular pigment xanthophyll," J. Biomed. Opt. **15**, 061714 (2010).
7. L. Kubecka, J. Jan, and R. Kolar, "Retrospective illumination correction of retinal images," Int. J. Biomed. Imaging **2010**, 780262 (2010).
8. J. Verdera, V. Caselles, M. Bertalmio, and G. Sapiro, "Inpainting surface holes," in *Proceedings of International Conference on Image Processing* (IEEE, 2003), pp. 903–906.
9. M. Bertalmio, G. Sapiro, V. Caselles, and C. Ballester, "Image inpainting," in *Proceedings of ACM Siggraph* (Addison-Wesley, 2000), pp. 417–424.
10. C. B. Schönlieb, "Applying modern PDE techniques to digital image restoration," http://www.mathworks.com/tagteam/71412_91992v00_applying-modern-pde-techniques-to-digital-image-restoration.pdf.
11. T. Chanwimaluang, G. Fan, and S. R. Fransen, "Hybrid retinal image registration," IEEE Trans. Inf. Technol. Biomed. **10**, 129–142 (2006).
12. S. Chaudhuri, S. Chatterjee, N. Katz, M. Nelson, and M. Goldbaum, "Detection of blood vessels in retinal images using two-dimensional matched filters," IEEE Trans. Med. Imag. **8**, 263–269 (1989).
13. A. Hoover, V. Kouznetsova, and M. Goldbaum, "Locating blood vessels in retinal images by piecewise threshold probing of a matched filter response," IEEE Trans. Med. Imag. **19**, 203–210 (2000).
14. C. Sinthanayothin, J. F. Boyce, H. L. Cook, and T. H. Williamson, "Automated localization of the optic disc, fovea, and retinal blood vessels from digital color fundus images," Br. J. Ophthalmol. **83**, 902–910 (1999).
15. A. D. Fleming, K. A. Goatman, S. Philip, J. A. Olson, and P. F. Sharp, "Automatic detection of retinal anatomy to assist diabetic retinopathy screening," Phys. Med. Biol. **52**, 331–345 (2007).
16. W. R. Tobler and S. Kennedy, "Smooth multidimensional interpolation," Geogr. Anal. **17**, 251–257 (1985).
17. W. Press, B. Flannery, S. Teukolsky, and W. T. Vetterling, *Numerical Recipes: The Art of Scientific Computing* (Press Syndicate, University Cambridge, 2007).
18. M. N. O. Sadiku, *Elements of Electromagnetics* (Sounders College, 2000).
19. E. Kreyszig, *Advanced Engineering Mathematics* (Wiley, 1993).
20. F. C. Delori, D. G. Goger, B. R. Hammond, D. M. Snodderly, and S. A. Burns, "Macular pigment density measured by autofluorescence spectrometry: comparison with reflectometry and heterochromatic flicker photometry," J. Opt. Soc. Am. A **18**, 1212–1230 (2001).
21. P. L. Kaufman and A. Alm, *Adler's Physiology of the Eye: Clinical Application* (Mosby, 2003).
22. J. d'Errico, "Inpaint nans," http://www.mathworks.com/matlabcentral/fileexchange/4551.
23. B. R. Hammond, Jr., B. R. Wooten, and D. M. Snodderly, "Individual variations in the spatial profile of human macular pigment," J. Opt. Soc. Am. A **14**, 1187–1196 (1997).
24. B. Dawant, A. Zijdenbos, and R. Margolin, "Correction of intensity variations in MR images for computer-aided tissue classification," IEEE Trans. Med. Imag. **12**, 770–781 (1993).
25. B. Likar, M. A. Viergever, and F. Pernuŝ, "Retrospective correction of MR intensity inhomogeneity by information minimization," IEEE Trans. Med. Imag. **20**, 1398–1410 (2001).
26. B. Nill and B. H. Bouzas, "Objective image quality measure derived from digital image power spectra," Opt. Eng. **31**, 813–825 (1992).